Applied Catalysis B: Environmental 320 (2023) 121981

Contents lists available at ScienceDirect

Applied Catalysis B: Environmental

journal homepage: www.elsevier.com/locate/apcatb

Engineering the surface chemical microenvironment over CuO nanowire arrays by polyaniline modification for efficient ammonia electrosynthesis from nitrate

You Xu, Yisheng Wen, Tianlun Ren, Hongjie Yu, Kai Deng, Ziqiang Wang, Xiaonian Li, Liang Wang *, Hongjing Wang *

State Key Laboratory Breeding Base of Green-Chemical Synthesis Technology, College of Chemical Engineering, Zhejiang University of Technology, Hangzhou 310014, PR China

ARTICLE INFO

Keywords:
CuO
Polyaniline
Ammonia electrosynthesis, Nitrate electroreduction, Surface chemical microenvironment

ABSTRACT

Electrochemical nitrate reduction into ammonia offers an attractive alternative to value-added ammonia (NH_3) production under benign conditions. The critical to achieve satisfactory NH_3 production rate from nitrate electroreduction that can compare with industrial Haber–Bosch route is the development of highly efficient electrocatalysts. In this work, we descript a post-modification strategy for synthesizing polyaniline (PANI)-modified CuO nanowire arrays (CuO@PANI) for selective electrocatalytic nitrate-to-ammonia transformation. Surface modification of CuO with PANI can not only well-retain the nanowire array structure and large specific surface area, but also modulate the surface chemical microenvironment of catalyst, which promotes nitrate enrichment and hydrogenated species accumulation, and thus facilitates selective nitrate-to-ammonia transformation. As a result, the CuO@PANI exhibits high Faradaic efficiency (93.88%) and excellent NH_3 selectivity (91.38%) for NH_3 electrosynthesis from nitrate. The strategy is worthy for designing high-efficiency electrocatalysts by surface modification with organic molecular or polymers for selective nitrate reduction into ammonia.

1. Introduction

Nitrogen is an essential element in human life and industry and its existing forms include nitrogen (N_2), ammonia (NH_3), nitrite (NO_2^-), nitrate (NO_3^-) and so on [1–3]. Among them, NH_3 is the most widely produced chemical with an annual production of over 200 million tons [4,5], which not only plays a very important role in manufacturing agricultural fertilizers and industrial productions, but also is regarded as the next generation energy carrier due to its high energy density (4.3 kw h kg^{-1}) and pollution-free [6–8]. Nowadays, NH_3 is almost outputted by the Haber–Bosch process with the N_2 and H_2 as reactant feeds [9]. However, the Haber–Bosch technology is energy-intensive, which consumes around 3%− 5% of the natural gas production, corresponding to about 1–2% annual energy supply of the world [10,11]. During the past decade, NH_3 production by means of electrocatalytic nitrogen reduction reaction with water as a hydrogen source has been an interesting topic [12,13]. But it is retarded by the high dissociation energy of N≡N bonds (941 kJ mol^{-1}) and the competitive hydrogen evolution reaction (HER), resulting in low NH_3 Faradaic efficiency (FE) [14–16]. Therefore, it is urgently desired to explore new avenues to achieve green NH_3 synthesis under benign conditions. On the other side, nitrate contamination of groundwater, which is mainly caused by the anthropogenic activities such as the use of nitrogen-based fertilizers in agriculture, is a widespread problem worldwide and poses a potential threat to public health [17,18]. Some physicochemical methods including electrodialysis [19], ion exchange[20] and reverse osmosis[21] have been employed to treat or remove nitrate contamination in wastewater. However, expensive post-treatment processes are always required as these physicochemical processes only separate and concentrate nitrate rather than completely destroy it, which may generate amounts of secondary brine wastes [22,23]. From the perspective of turning waste into wealth, it is attractive to convert nitrate contamination in wastewater into recyclable ammonia, especially via electroreduction using water as a hydrogen source under mild conditions.

Electrochemical nitrate reduction to ammonia is limited by the competitive HER and the complex eight-electron, nine-proton reduction

* Corresponding authors.
E-mail addresses: wangliang@zjut.edu.cn (L. Wang), hjw@zjut.edu.cn (H. Wang).

https://doi.org/10.1016/j.apcatb.2022.121981
Received 9 April 2022; Received in revised form 9 September 2022; Accepted 11 September 2022
Available online 13 September 2022

process [24–28]. Hence, the development of highly efficient electrocatalysts is necessary for the application of electrochemical nitrate-to-ammonia conversion technology. Recent achievements have highlighted the unique superiority of Cu-based materials for selective electrocatalytic nitrate reduction to ammonia [29–34]. In order to achieve high performance, much efforts have been made to regulate the active sites of electrocatalysts by precisely sharpening the morphologies and structures, and tuning the compositions. Among various nanostructures, 1D nanowire arrays have been proved to be superior for electrocatalysis with the advantages of the abundant, exposed active sites and efficient charge transfer [35,36]. In addition, surface modification of heterogeneous electrocatalysts, especially using organic molecular or polymers, has emerged as an effective way to boost their electrocatalytic activity [37–40]. For example, the polyethylenimine (PEI) functionalized Au nanowires@Pd core-shell bimetallic nanohybrids (Au-NWs@Pd@PEI) exhibit superior electrocatalytic performance toward oxygen reduction reaction due to the -NH_2 functional group of PEI [41], and the tannic acid (TA) coordinated with different metal ions shows outstanding electrocatalytic performance due to the synergy between the composite coatings to achieve favorable surface performance adjustments [42,43]. Despite these advances, there are few studies to date concern selectively electroreduction of nitrate to ammonia by surface molecular or polymers functionalization.

Herein, we developed a post-modification strategy for synthesizing polyaniline (PANI) modified CuO nanowire arrays supported on copper foam (CuO@PANI/CF) as a self-supported electrocatalyst for selective nitrate electroreduction to ammonia. Rational surface modification of CuO nanowire arrays with PANI could not only well-retain the nanowire array structure, more importantly, modulate the surface chemical microenvironment of catalyst. The constructed CuO@PANI hybrid structures show following advantages: (i) PANI with lone electron pairs on N atoms is able to capture proton from hydronium ions and forms a positively charged surface, which facilitates the enrichment and fixation of NO_3^- anions on the catalyst surface; (ii) Protonated amine groups in PANI layer have high positive charge density and can be electro-reduced easily to form adsorbed H atom (*H), which is key hydrogenated species during nitrate-to-ammonia conversion; (iii) The hierarchical structure of CuO@PANI nanowire arrays favors the mass transportation/diffusion during nitrate reduction electrocatalysis; (iv) The electronic interactions between PANI and CuO in CuO@PANI can achieve high conductivity and accelerate electron transfer for the electrocatalysis reaction. With these advantages, the resultant self-supported CuO@PANI/CF electrode exhibited enhanced electrocatalytic nitrate-to-ammonia capability (NH_3 FE: 93.88%, NH_3-N selectivity: 91.38%, NH_3 yield rate: 0.213 mmol h^{-1} cm^{-2}), which is superior to the pristine un-modified CuO nanowire arrays supported on Cu foam (CuO/CF) (NH_3 FE:89.14%, NH_3-N selectivity: 79.73%, NH_3 yield rate: 0.185 mmol h^{-1} cm^{-2}).

2. Experimental

2.1. Synthesis of CuO/CF

Firstly, a piece of Cu foam (2 cm × 1 cm) was cleaned by hydrochloric acid (3 M) for 30 min under ultrasonic bath, followed by washing with ethanol and deionized water several times. Next, the Cu foam was placed upright in a 8 ml mixture solution containing $(NH_4)_2S_2O_8$ (0.05 mol L^{-1}) and NaOH (1 mol L^{-1}) for 30 min at room temperature, generating $Cu(OH)_2$ nanowires arrays supported on Cu foam substrate ($Cu(OH)_2$/CF) [44]. CuO NAs/CF was achieved by calcining the as-prepared $Cu(OH)_2$/CF at 200 °C for 2 h under N_2 atmosphere with a temperature increase rate of 1 °C min^{-1}.

2.2. Synthesis of CuO@PANI/CF

The PANI layer was modified on the surface of CuO NAs/CF by electrodeposition in solution of aniline (0.01 M) and Na_2SO_4 (50 mM) at 0.5 mA cm^{-2} for 500 s at room temperature [45]. The obtained CuO@PANI/CF composite was washed by deionized water for four times.

2.3. Synthesis of PANI/CF

PANI coated on the surface of bare Cu foam (PANI/CF) was manufactured by the same method as CuO@PANI/CF, except that blank Cu foam was used as the substrate for electrodeposition.

2.4. Electrochemical measurements

Electrocatalytic nitrate reduction reaction (NO_3RR) measurements were performed by using an electrochemical workstation (CHI 660D, CH Instruments, USA) in a standard three-electrode system, where CuO@PANI/CF (1 cm × 1 cm), Pt foil and saturated calomel electrode (SCE) were used as the working electrode, counter electrode and reference electrode, respectively. 35 ml of 0.5 M K_2SO_4 solution was added to the cathode and anode chamber, respectively. The performance of NO_3RR was studied by adding additional KNO_3 (200 ppm NO_3^--N) to the cathode chamber. Prior the NO_3^- reduction test, the electrolyte was purged with Ar (99.99% purity) for 15 min and then performed linear scanning voltammetry (LSV) measurements at 10 mV s^{-1} for several times until a steady state was achieved. Chronoamperometry (i-t) tests were conducted at different applied potentials under stirring (stirring rate: 350 rpm) for 2 h to investigate the electrocatalytic NO_3RR activity. The concentrations of nitrate, nitrite, and ammonia are determined according to the reported colorimetric methods, see detailed information in the Supplementary Material. Electrochemical impedance spectroscopy (EIS) measurements were performed in a 0.5 M K_2SO_4 solution containing 200 ppm of nitrate at − 0.95 V (vs. SCE), with the frequency range of 0.1 Hz ~100 kHz and the AC amplitude of 5 mV. For comparison, the bare Cu foam, PANI/CF and CuO/CF were employed as contrastive catalysts for electrochemical study. Cyclic voltammetry (CV) curves in the electrochemical double layer capacitance (C_{dl}) determination were measured at different scan rates of 30, 40, 50, 60, 70 mV s^{-1}, respectively.

3. Results and discussion

3.1. Synthesis and physicochemical characterization of CuO@PANI/CF

The synthesis of CuO@PANI/CF was schematically illustrated in Fig. 1. Firstly, $Cu(OH)_2$ nanowire arrays grown on Cu foam substrate (denoted as $Cu(OH)_2$/CF) was obtained by a wet-chemical method [44]. Next, the in-situ conversion of $Cu(OH)_2$/CF to CuO/CF was achieved by calcination at 200 °C under N_2 atmosphere. Unlike bare CF with smooth surface (Fig. S1), dense and uniform CuO nanowire array structures can be observed in the CuO/CF sample, shown in Fig. S2. Then, PANI was electrodeposited on the surface of CuO nanowires, generating the CuO@PANI/CF composite.

Scanning electron microscope (SEM) images of the typical CuO@PANI/CF are shown in Fig. 2a-b and Fig. S3. The nanowire structure vertically supported on the CF substrate is maintained after the surface is modified with PANI and the length of these nanowires is about 6–8 μm. As a comparative sample, the bare CF modified with PANI (denoted as PANI/CF) was also synthesized by the similar electrodeposition method (Fig. S4). To gain more detailed structural information, some CuO@PANI nanowires were scraped off from Cu foam substrate and subjected to transmission electron microscopy (TEM) characterization. TEM image in Fig. 2c reveals the rough surface of these nanowire structures and the diameter of the CuO nanowires is approximately 130 nm. From the high-resolution TEM (HRTEM) image, a thin amorphous PANI layer on the edge of the nanowire with a thickness of 2–3 nm can be observed, which implies that PANI is successfully modified on the surface of CuO nanowires (Fig. 2d). Simultaneously, the *d*-spacing of the crystal lattices of

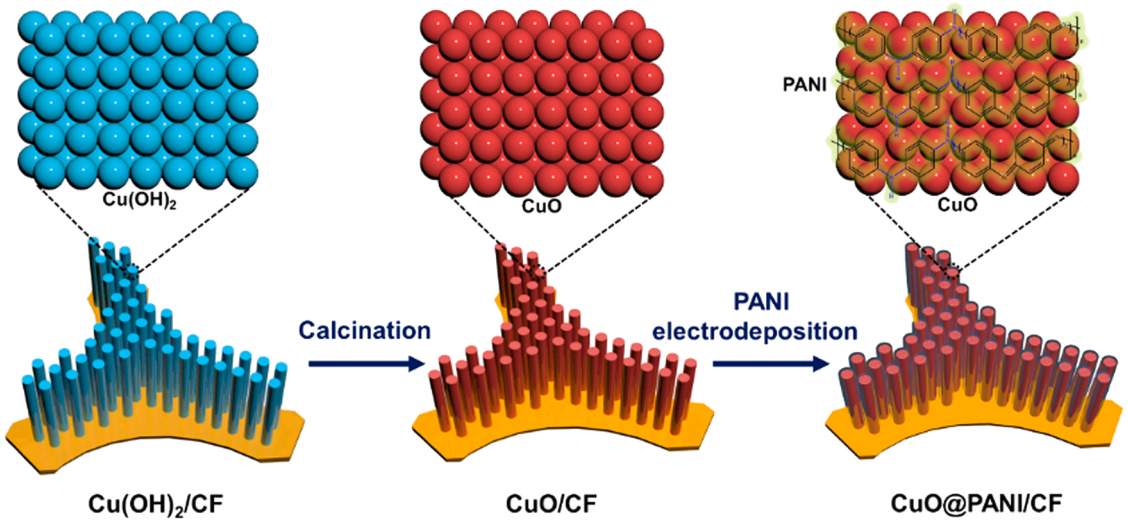

Fig. 1. Schematic illustration for the preparation of CuO@PANI/CF composite.

0.252 nm and 0.253 nm could be assigned to (11−1) plane and (002) plane of CuO, respectively. To further analyze the element composition and distribution of CuO@PANI nanowires, high-angle annular dark-field scanning transmission electron microscopy (HAADF-STEM) and corresponding element mappings were acquired. As displayed in Fig. 2e, Cu, O, C and N elements are uniformly distributed throughout the nanowire.

X-ray diffraction (XRD) was performed to characterize the crystal structure of the samples. Fig. 3a presented the XRD patterns of CuO@PANI nanowires and CuO nanowires. Obviously, the CuO nanowires show typical XRD pattern of monoclinic CuO (JCPDS NO. 48–1548). After surface modification with PANI, the crystal structure of CuO did not change. Fourier transform infrared spectroscopy (FTIR) was employed to further verify the formation of the PANI modified on the surface of CuO nanowires (Fig. 3b). Compared with pristine un-modified CuO nanowires, the CuO@PANI nanowires show several characteristic peaks of PANI, which can be assigned to the stretching mode of N = G=N (G = quinone) at 1060 cm^{-1} and 1112 cm^{-1}, C=C stretching of benzoid units (1461 cm^{-1}) and the N-H bond of the aromatic amine moieties (2923 cm^{-1} and 2956 cm^{-1}) of PANI [46,47]. Besides, C=C stretching of quinoid rings shifted from 1569 cm^{-1} to 1616 cm^{-1} may be caused by the formation of hydrogen bonding between CuO and the NH group of PANI [48]. X-ray photoelectron spectroscopy (XPS) investigation was further conducted to analyze the surface compositions and valence states. The XPS survey spectrum reveals that CuO@PANI nanowires are composed of Cu, O, C and N species (Fig. S5). The Cu 2p spectrum of CuO@PANI nanowires displays two prominent peaks for Cu^{2+} $2p_{3/2}$ and Cu^{2+} $2p_{1/2}$ at 933.46 eV and 953.4 eV, respectively, with associated satellite peaks at 942.1 eV and 961.98 eV (Fig. 3c) [49,50]. In the O 1 s spectra (Fig. 3d), two major peaks at 529.59 eV and 531.23 eV are attributed to Cu-O linkage and surface adsorbed hydroxyl ions [49]. The N 1 s spectra, as shown in Fig. 3e, can be divided into imine-like structure (-C=N-), neutral amine-like structure(-NH-), and charged structure(-NH^+-) with the corresponding peaks at 398.6 eV, 399.7 eV, 400.7 eV, respectively [51,52]. Further, the C-C (284.4 eV), C-N (285.2 eV) and C-O (288.2 eV) can be observed from the C 1 s spectra (Fig. 3f) [53]. Combined with the characterization results of FTIR and XPS, it is confirmed that PANI is successfully generated on the surface of CuO nanowires. Zeta potential measurements were carried out to characterize the electrical charge on the surface of nanowire arrays. Pristine CuO nanowires show a zeta potential of − 17.3 mV. With surface PANI modification, the zeta potential changes from negative to positive (+2.58 mV) (Fig. S6). It is believed electrostatic attraction between positively charged CuO@PANI nanowires and negatively charged nitrate ions facilitate the accumulation of nitrate ions on the surface of CuO@PANI nanowires.

3.2. Electrocatalytic NO_3RR performance over the CuO@PANI/CF

Electrochemical NO_3RR measurements were tested in a H-type electrolytic cell with a three-electrode system composed of CuO@PANI/NF, Pt foil and SCE as the working, counter and reference electrodes, respectively (Fig. S7). After electroreduction, the electrolyte was diluted with a certain ratio and then determined by ultraviolet-visible (UV-Vis) spectrophotometry to determine the concentration of NO_3^--N, NO_2^--N and NH_3-N on the basis of the calibration curves (Fig. S8). LSV curves recorded in the electrolyte with or without nitrate using CuO@PANI/CF working electrode show obvious discrepancy from − 0.8 V to − 1.7 V (vs. SCE) (Fig. 4a), suggesting the participation of NO_3^- in the electroreduction process. Furthermore, a series of potentials from − 1.1 V to − 1.5 V (vs. SCE) were performed to investigate the catalytic properties of CuO@PANI/CF for NO_3RR. The conversion efficiency of NO_3^--N reaches the highest value (97.16%) at − 1.3 V (vs. SCE), and then tends to stabilize (Fig. 4b). Meanwhile, as shown in the Fig. 4c-e, the yield rate, FE and selectivity of NH_3, at the applied potential of 1.3 V (vs. SCE), achieve maximum values (0.213 mmol h^{-1} cm^{-2}, 93.88%, 91.38%), while the catalytic performance gradually decreases with the potential negatively increases due to the competitive reaction (i.e., HER). It is worth noting that only 2.19% of the NO_2^--N and 6.43% of other by-products (e.g., N_2, NO_x, etc.) can be detected in the post-electrolysis electrolyte, indicating that the CuO@PANI/CF has excellent ammonia selectivity. When performing NO_3RR, the anodic half-reaction is the oxygen evolution reaction (OER). The generate O_2 at Pt foil counter electrode during NO_3RR electrolysis at 1.3 V (vs. SCE) for 2 h was collected by drainage method and the oxygen evolution rate was calculated to 0.621 mmol h^{-1} cm^{-2}, with a O_2 FE closed to 100%. Moreover, the changes in the concentration of NO_3^--N, NO_2^--N and NH_3-N under different reaction times were investigated. As displayed in the Fig. 4f, with prolonged electrolysis time, the concentration of NO_3^--N continuously decreases, while the concentration of NH_3-N increases. Moreover, as the first product and main quasi-stable intermediate of nitrate reduction[54], the concentration of NO_2^--N increase in the first 15 min, then decreases gradually with reaction time, because most of generated NO_2^- intermediate would be further reduced either directly to NH_3 or indirectly to N_2 via several intermediates. In addition, CuO@PANI/CF can also express higher NH_3-N selectivity and NO_3^--N conversion rate at higher NO_3^--N concentrations (Fig. S9). Impressively, the NO_3RR performance of CuO@PANI/CF for ammonia synthesis is better than many other reported catalysts (Table S1).

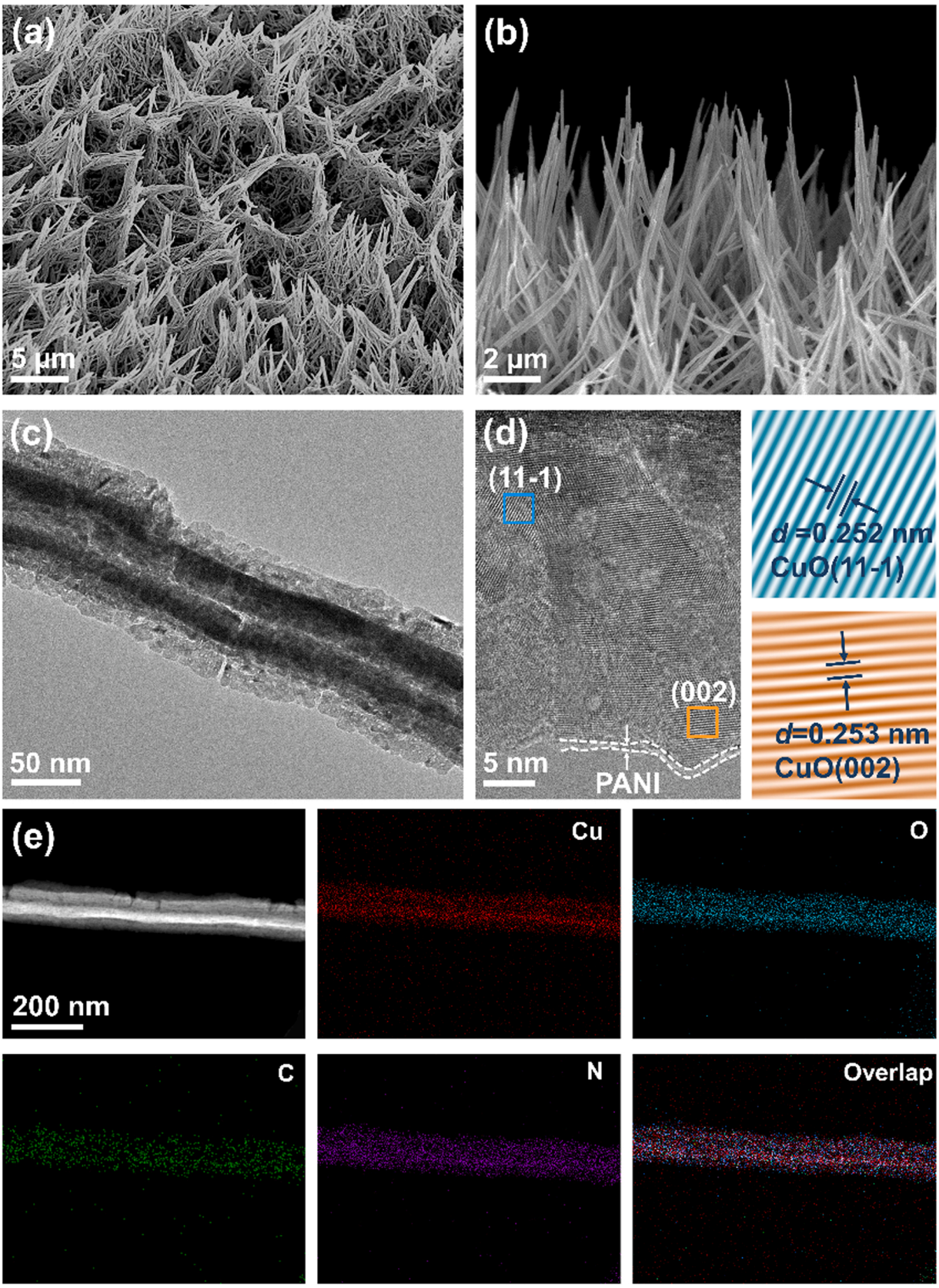

Fig. 2. (a) Low and (b) high magnification SEM images of CuO@PANI/CF. (c) TEM image, (d) HRTEM image, (e) HAADF-STEM image and element mapping images of CuO@PANI nanowires.

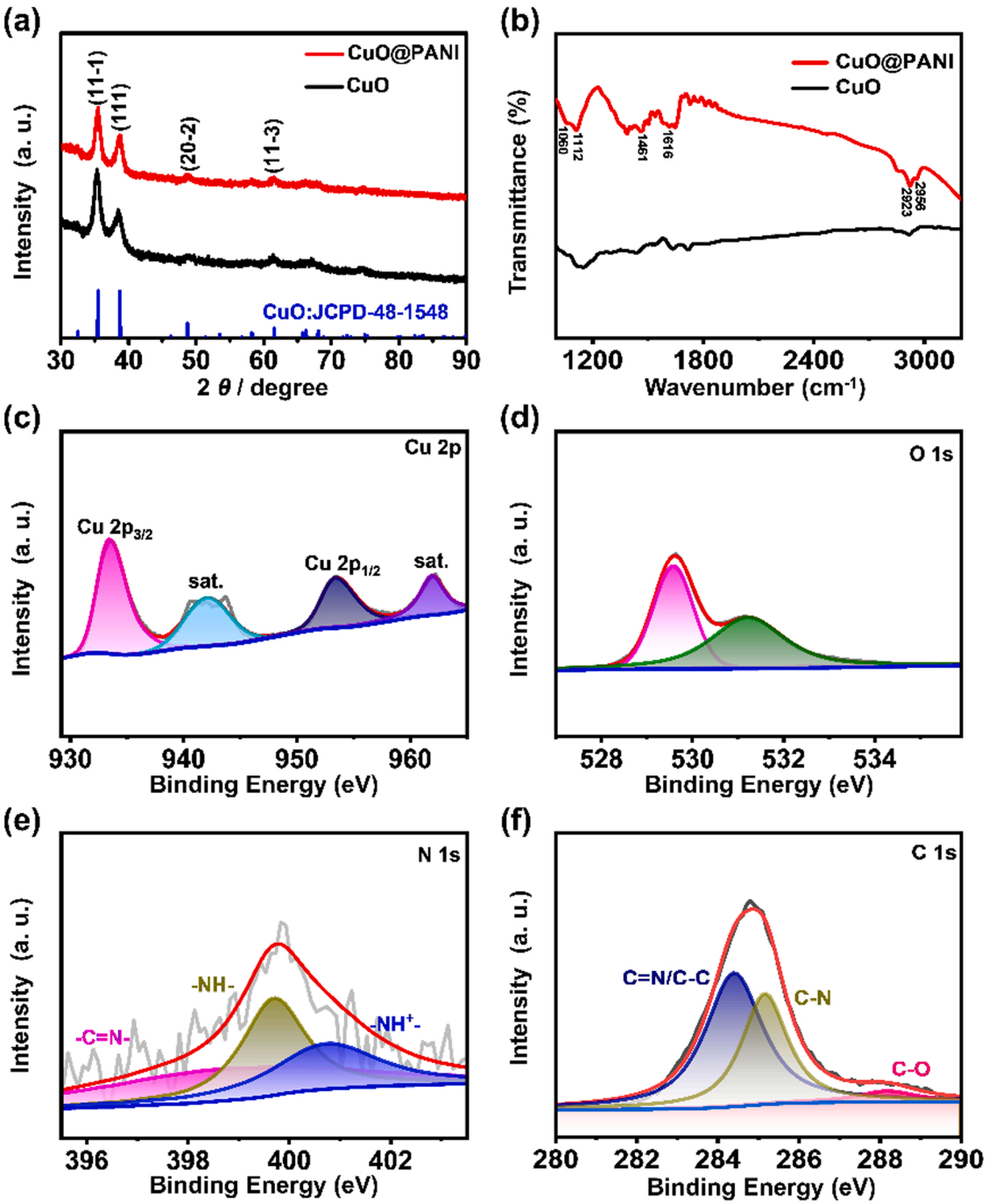

Fig. 3. (a) XRD patterns of CuO@PANI nanowires and CuO nanowires. (b) FT-IR spectra of CuO@PANI nanowires and CuO nanowires. (c) Cu 2p XPS spectrum, (d) O 1 s XPS spectrum, (e) N 1 s XPS spectrum and (f) C 1 s XPS spectrum of CuO@PANI nanowires.

In order to explore the effect of surface functionalization and microstructure on the electrocatalytic performance for NO_3RR, pure Cu foam (CF), PANI/CF and CuO/CF were used for contrast test. The LSV curves of CuO@PANI NAs/CF show a higher current density than those of other contrastive samples (Fig. S10). Besides, the comparison of NO_3RR performance at − 1.3 V (vs. SCE) is shown in Fig. 5a-d. Obviously, the CuO@PANI/CF exhibits the best catalytic activity for NO_3RR relative to pure CF (NO_3^--N conversion rate: 10.81%, NH_3-N selectivity: 19.33%, FE: 16.36%, NH_3 yield rate: 0.005 mmol h^{-1} cm^{-2}), PANI/CF (52.87%, 21.65%, 50.46%, 0.028 mmol h^{-1} cm^{-2}) and CuO/CF (96.65%, 79.73%, 89.14%, 0.185 mmol h^{-1} cm^{-2}), confirming that the synergistic effect of CuO and PANI can effectively enhance the catalytic activity of nitrate electroreduction. The active sites of CuO@PANI/CF for NO_3RR are related to the electrochemical active surface areas (ECSA). The C_{dl} measurement was carried out to determine the ECSA, as the C_{dl} value of electrocatalyst is proportional to its ECSA [55–57]. As shown in the Fig. S11, the ECSA of 124.25 cm^2 can be calculated for CuO@PANI/CF (according to the equation: ECSA = C_{dl}/0.04 mF cm^{-2} per cm^2), which is higher than that of CuO/CF (30.25 cm^2). Furthermore, the measurement results of the EIS suggest that the CuO@PANI/CF has lower electron transfer resistance than CuO/CF (Fig. S12), suggesting faster electron transfer kinetics. These results indicate that PANI endows abundant catalytic active sites on the CuO surface due to the presence of the amino and imino functional groups, which can enhance the NO_3^- adsorption and hydrogenation process. Simultaneously, as a conductive polymer, the modification of PANI can further

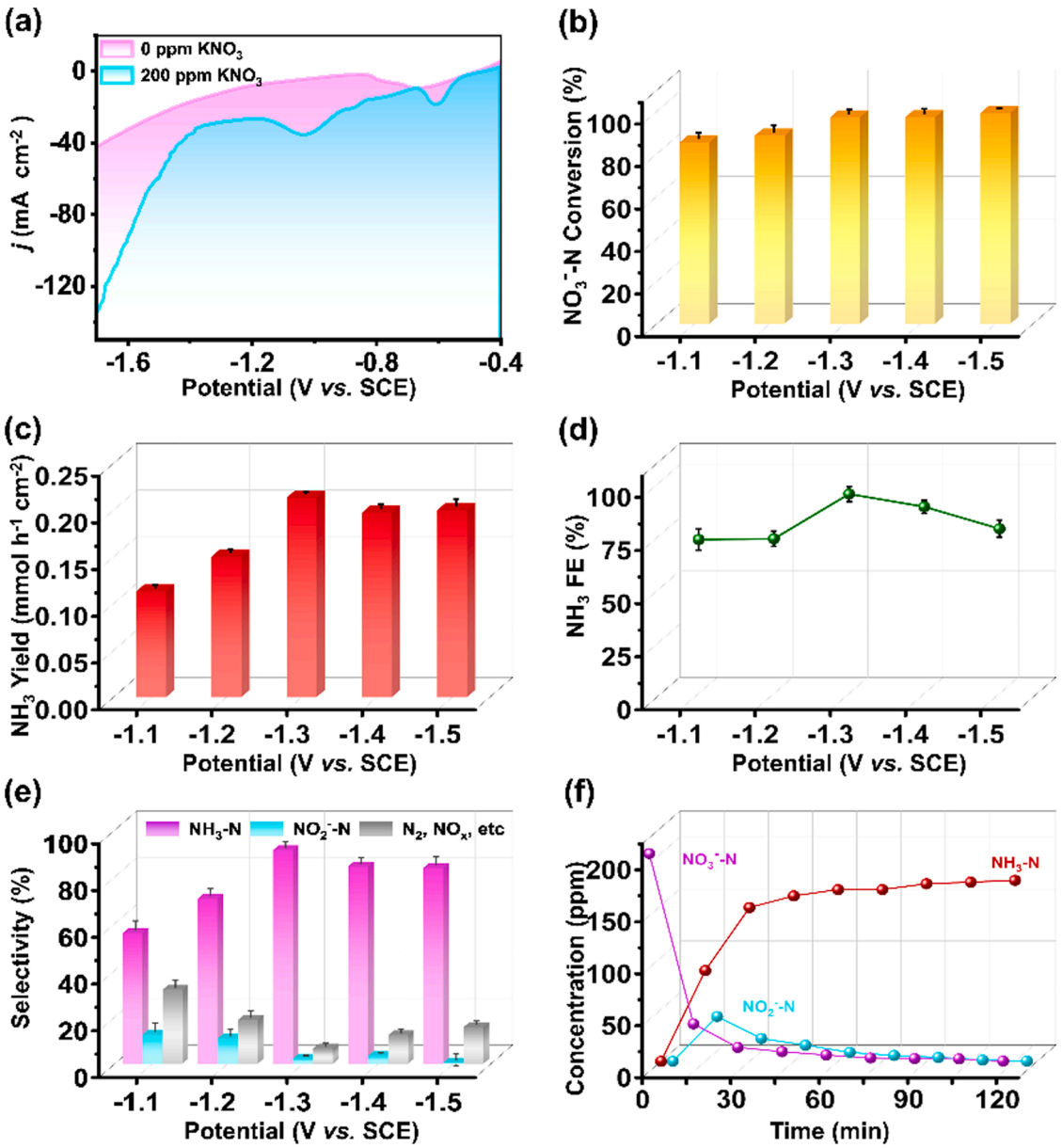

Fig. 4. (a) LSV curves of CuO@PANI/CF in 0.5 M K_2SO_4 solution with or without nitrate. (b) NO_3^--N conversion, (c) NH_3 yield rate, (d) Faradaic efficiency and (e) product selectivities of CuO@PANI/CF at various applied various potentials. (f) Time-dependent concentration of NO_3^--N, NO_2^--N and NH_3-N for CuO@PANI/CF at − 1.3 V (vs. SCE).

improve the conductivity, thereby accelerating the electron transfer rate. To unveil the activity origin of the cathodic catalyst, CuO@PANI nanowires after NO_3RR testing were characterized by XRD. As presented in Fig. S13, unlike initial CuO@PANI, the diffraction peaks of $Cu_{2+1}O$ phase (Cu_2O with metal excess defects [58,59], JCPDS NO. 05–0667) and Cu phase (JCPDS NO. 04–0836) can be observed in the post-NO_3RR CuO@PANI. The characterization results of XRD imply the initial CuO phase was in-situ electrochemically reduced into $Cu/Cu_{2+1}O$ hetero-phase structure under nitrate electroreduction operating conditions, during which the whole nanowire array structure was well maintained [60].

The same CuO@PANI/CF electrode was continuously recycled five times to measure the electrocatalytic stability at − 1.3 V (vs. SCE). The NH_3-N yield rate, NO_3^--N conversion efficiency and FE basically stabilized and fluctuated in a small range during the five cycles, indicating the good catalytic stability for NO_3RR (Fig. 6a and b). Additionally, the NH_3-N selectivity showed no significant decay during the continuous recycling measurement for 5 cycles (Fig. S14). The SEM and TEM characterization results display that the nanowire array structure is maintained (Fig. S15a-d), even if CuO phase has been electrochemically converted into $Cu/Cu_{2+1}O$ phase. Furthermore, the existence of PANI is also confirmed by the appearance of C and N elements in the element mapping images (Fig. S15e). To exclude the influence of external experimental conditions on ammonia synthesis, we conducted a comparison test with the blank K_2SO_4 solution as reactant, which produces ignorable ammonia after test, confirming that the ammonia mainly comes from nitrate electroreduction (Fig. S16). To further verify the source of ammonia, ^{15}N isotope labeling experiments were conducted using $K^{15}NO_3$ as the source of nitrogen. The ^1H proton nuclear magnetic resonance spectra (^1H NMR) of electrolyte after electrochemical reduction of $K^{15}NO_3$ show typical double peaks at $\delta = 6.88$ and $\delta = 7.07$ ppm, which is consistent with the standard sample of $^{15}NH_4Cl$, and the ^1H NMR spectra of electrolyte adopting $K^{14}NO_3$ as reactants shows triple peaks of $^{14}NH_4^+$ (Fig. 6c). Considering that the peak area of

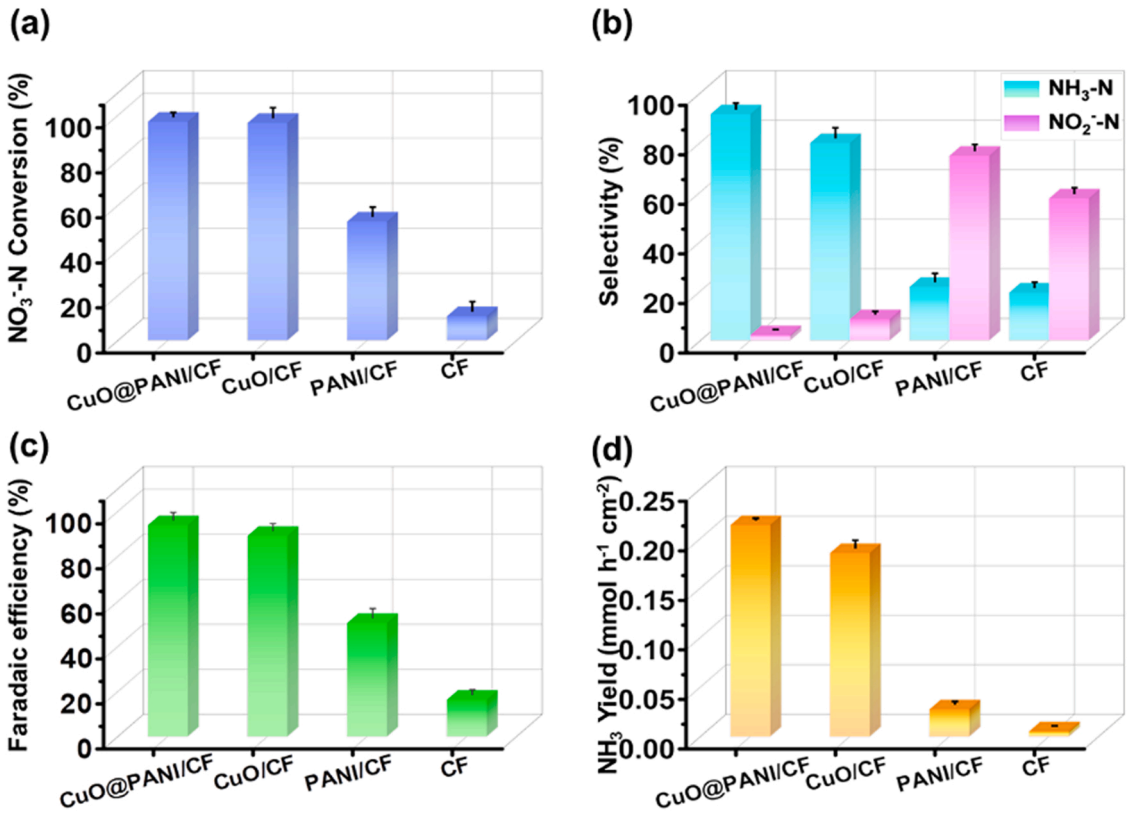

Fig. 5. (a) NO_3-N conversion. (b) NH_3-N and NO_2-N selectivity. (c) Faradaic efficiency and (d) NH_3 yield rate of different samples.

^{1}H NMR is linked to the ammonia content, the NH_3 concentration is further quantified by ^{1}H NMR with external standards of maleic acid (Fig. S17). The $^{15}NH_4^+$-^{15}N is so close to the colorimetric method result (Fig. 6d), These results demonstrates that the produced ammonium is completely originated from nitrate.

3.3. *Investigation of performance enhancement mechanisms*

The possible mechanism of CuO@PANI/CF towards nitrate reduction to ammonia is shown in the Fig. 6e. Nanowire arrays supported on the Cu foam could provide a large of active sites and efficient mass transfer for electrochemical reactions. The CuO phase in initial CuO@PANI/CF was in-situ converted into Cu/$Cu_{2+1}O$ hetero-phase structure under NO_3RR operating conditions. Both Cu and $Cu_{2+1}O$ serve as active sites in NO_3RR electrocatalysis, in which the $Cu_{2+1}O$ site could activate and reduce nitrate and the Cu site could promote the reduction of protons to adsorbed H atom (*H) to boost nitrate hydrogenation kinetics. According to the previous reports, electron transfer at the interface of Cu/CuO_x is beneficial to the formation of some key reaction intermediates during nitrate electroreduction process and suppresses the competitive cathodic HER [60,61]. Surface modification with PANI could modulate the surface chemical microenvironment of CuO nanowire arrays and provide positively charged catalytic surface, which largely facilitating the adsorption of nitrate ions due to electrostatic interaction [62,63]. The nitrate ions would further migrate to $Cu_{2+1}O$ site and are electro-reduced to ammonia via a series of deoxidation and hydrogenation reactions. Moreover, protonated amine groups in PANI could capture protons from hydrated ions to form protonated amino groups and the captured protons would be further be electro-reduced by Cu sites to form *H [46], which is key hydrogenated species during nitrate-to-ammonia conversion. Accumulation of hydrogenated species at the active sites is conducive to promote the ammonia formation reaction pathway, thus improve the selectivity of NH_3 and limit the formation of other byproducts at the same time. Simultaneously, the externally modified PANI, as a conductive polymer, could achieve high conductivity and accelerate electron transfer for the electrocatalysis reaction [64].

4. Conclusions

In summary, CuO@PANI nanowire arrays were synthesized via a post-modification strategy and used as an active electrocatalyst for NO_3RR. A series of characterization and electrochemical studies demonstrated that surface modification of CuO with PANI could not only well-retain the nanowire array structure, more importantly, modulate the surface chemical microenvironment, thus promote the enrichment of nitrate ions and hydrogenated species on the catalytic surface. In addition, PANI as a conductive polymer improves the conductivity of the catalyst and accelerates electron transfer. The as-prepared CuO@PANI/CF exhibited an excellent performance for ammonia synthesis from nitrate electroreduction with the NO_3-N conversion rate (97.16%), NH_3-N selectivity (91.38%), FE (93.88%) and the NH_3 yield rate (0.213 mmol h^{-1} cm^{-2}) at − 1.3 V (vs. SCE), which are higher than CuO/CF and other contrastive samples. This work provides a new way to construct efficient electrocatalysts for the selective conversion of nitrate to ammonium through organic polymers modification.

CRediT authorship contribution statement

You Xu: Investigation, Writing – original draft, Funding acquisition. **Yisheng Wen:** Data curation, Investigation. **Tianlun Ren:** Formal analysis, Data curation. **Hongjie Yu:** Data curation, Funding acquisition. **Kai Deng:** Validation, Investigation. **Ziqiang Wang:** Validation, Funding acquisition. **Xiaonian Li:** Resources, Methodology. **Liang Wang:** Project administration, Writing – review & editing, Funding acquisition. **Hongjing Wang:** Supervision, Writing – review & editing, Funding acquisition.

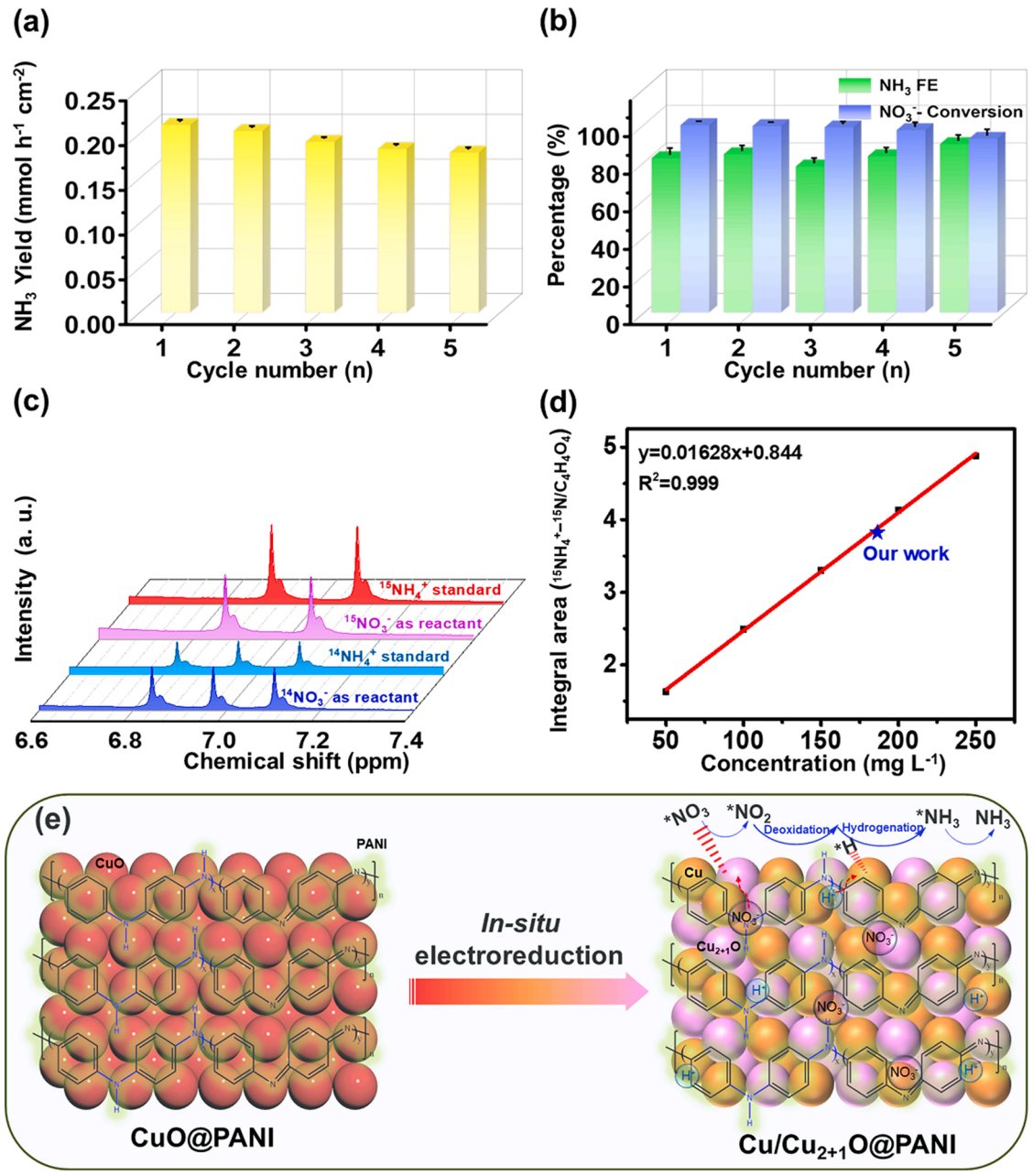

Fig. 6. (a) NH_3 yield rate, (b) NO_3^--N conversion and Faradaic efficiency measured for 5 cycles at − 1.3 V (vs. SCE) with the same piece of catalyst. (c) The ^1H NMR spectra of $^{15}NH_4^+$ and $^{14}NH_4^+$ calibration solutions, and ^1H NMR spectra of electrolytes after electrocatalytic nitrate reduction employing $^{15}NO_3^-$ and $^{14}NO_3^-$ as nitrogen sources. (d) The standard curve of integral area ($^{15}NH_4^+-^{15}N/C_4H_4O_4$) against $^{15}NH_4^+-^{15}N$ concentration. (e) Schematic illustrating the mechanism of electrocatalytic nitrate reduction to ammonia on CuO@PANI/CF.

Declaration of Competing Interest

The authors declare that they have no known competing financial interests or personal relationships that could have appeared to influence the work reported in this paper.

Data Availability

Data will be made available on request.

Acknowledgements

This work was financially supported by the National Natural Science Foundation of China (Nos. 21701141, 21972126, 21978264, 21905250 and 22278369), China Postdoctoral Science Foundation (2021M702889), and Natural Science Foundation of Zhejiang Province (No. LQ22B030012).

Appendix A. Supporting information

Supplementary data associated with this article can be found in the online version at doi:10.1016/j.apcatb.2022.121981.

References

[1] Y.-C. Hao, Y. Guo, L.-W. Chen, M. Shu, X.-Y. Wang, T.-A. Bu, W.-Y. Gao, N. Zhang, X. Su, X. Feng, J.-W. Zhou, B. Wang, C.-W. Hu, A.-X. Yin, R. Si, Y.-W. Zhang, C.-H. Yan, Promoting nitrogen electroreduction to ammonia with bismuth

nanocrystals and potassium cations in water, Nat. Catal. 2 (2019) 448–456, https://doi.org/10.1038/s41929-019-0241-7.
[2] L. Li, Y. Wang, S. Vanka, X. Mu, Z. Mi, C.J. Li, Nitrogen photofixation over III-nitride nanowires assisted by ruthenium clusters of low atomicity, Angew. Chem. Int. Ed. 56 (2017) 8701–8705, https://doi.org/10.1002/anie.201703301.
[3] C. Tang, S.Z. Qiao, How to explore ambient electrocatalytic nitrogen reduction reliably and insightfully, Chem. Soc. Rev. 48 (2019) 3166–3180, https://doi.org/10.1039/c9cs00280d.
[4] X. Deng, Y. Yang, L. Wang, X.Z. Fu, J.L. Luo, Metallic Co nanoarray catalyzes selective NH3 production from electrochemical nitrate reduction at current densities exceeding 2 A cm(-2), Adv. Sci. 8 (2021) 2004523, https://doi.org/10.1002/advs.202004523.
[5] L. Li, C. Tang, D. Yao, Y. Zheng, S.-Z. Qiao, Electrochemical nitrogen reduction: identification and elimination of contamination in electrolyte, ACS Energy Lett. 4 (2019) 2111–2116, https://doi.org/10.1021/acsenergylett.9b01573.
[6] Y. Guo, R. Zhang, S. Zhang, Y. Zhao, Q. Yang, Z. Huang, B. Dong, C. Zhi, Pd doping-weakened intermediate adsorption to promote electrocatalytic nitrate reduction on TiO_2 nanoarrays for ammonia production and energy supply with zinc–nitrate batteries, Energy Environ. Sci. 14 (2021) 3938–3944, https://doi.org/10.1039/d1ee00806d.
[7] L. Li, C. Tang, B. Xia, H. Jin, Y. Zheng, S.-Z. Qiao, Two-dimensional mosaic bismuth nanosheets for highly selective ambient electrocatalytic nitrogen reduction, ACS Catal. 9 (2019) 2902–2908, https://doi.org/10.1021/acscatal.9b00366.
[8] Y. Wan, H. Zhou, M. Zheng, Z.H. Huang, F. Kang, J. Li, R. Lv, Oxidation state modulation of bismuth for efficient electrocatalytic nitrogen reduction to ammonia, Adv. Funct. Mater. 31 (2021) 2100300, https://doi.org/10.1002/adfm.202100300.
[9] P.H. van Langevelde, I. Katsounaros, M.T.M. Koper, Electrocatalytic Nitrate Reduction for Sustainable Ammonia Production, Joule 5 (2021) 290–294, https://doi.org/10.1016/j.joule.2020.12.025.
[10] J. Li, Y. Zhang, C. Liu, L. Zheng, E. Petit, K. Qi, Y. Zhang, H. Wu, W. Wang, A. Tiberj, X. Wang, M. Chhowalla, L. Lajaunie, R. Yu, D. Voiry, 3.4% solar-to-ammonia efficiency from nitrate using Fe single atomic catalyst supported on MoS_2 nanosheets, Adv. Funct. Mater. (2021) 2108316, https://doi.org/10.1002/adfm.202108316.
[11] L. Wang, M. Xia, H. Wang, K. Huang, C. Qian, C.T. Maravelias, G.A. Ozin, Greening Ammonia toward the Solar Ammonia Refinery, Joule 2 (2018) 1055–1074, https://doi.org/10.1016/j.joule.2018.04.017.
[12] Y. Ren, C. Yu, X. Tan, H. Huang, Q. Wei, J. Qiu, Strategies to suppress hydrogen evolution for highly selective electrocatalytic nitrogen reduction: challenges and perspectives, Energy Environ. Sci. 14 (2021) 1176–1193, https://doi.org/10.1039/d0ee03596c.
[13] B. Yang, W. Ding, H. Zhang, S. Zhang, Recent progress in electrochemical synthesis of ammonia from nitrogen: strategies to improve the catalytic activity and selectivity, Energy Environ. Sci. 14 (2021) 672–687, https://doi.org/10.1039/d0ee02263b.
[14] M.A. Legare, G. Belanger-Chabot, R.D. Dewhurst, E. Welz, I. Krummenacher, B. Engels, H. Braunschweig, Nitrogen fixation and reduction at boron, Science 359 (2018) 896–899, https://doi.org/10.1126/science.aaq1684.
[15] Y. Pang, C. Su, G. Jia, L. Xu, Z. Shao, Emerging two-dimensional nanomaterials for electrochemical nitrogen reduction, Chem. Soc. Rev. 50 (2021) 12744–12787, https://doi.org/10.1039/d1cs00120e.
[16] J. Wang, L. Yu, L. Hu, G. Chen, H. Xin, X. Feng, Ambient ammonia synthesis via palladium-catalyzed electrohydrogenation of dinitrogen at low overpotential, Nat. Commun. 9 (2018) 1795, https://doi.org/10.1038/s41467-018-04213-9.
[17] Y. Wang, C. Wang, M. Li, Y. Yu, B. Zhang, Nitrate electroreduction: mechanism insight, in situ characterization, performance evaluation, and challenges, Chem. Soc. Rev. 50 (2021) 6720–6733, https://doi.org/10.1039/d1cs00116g.
[18] T. Zhu, Q. Chen, P. Liao, W. Duan, S. Liang, Z. Yan, C. Feng, Single-atom Cu catalysts for enhanced electrocatalytic nitrate reduction with significant alleviation of nitrite production, Small 16 (2020) 2004526, https://doi.org/10.1002/smll.202004526.
[19] D. Xu, Y. Li, L. Yin, Y. Ji, J. Niu, Y. Yu, Electrochemical removal of nitrate in industrial wastewater, Front. Environ. Sci. Eng. 12 (2018) 9, https://doi.org/10.1007/s11783-018-1033-z.
[20] M. Alikhani, M.R. Moghbeli, Ion-exchange polyHIPE type membrane for removing nitrate ions: preparation, characterization, kinetics and adsorption studies, Chem. Eng. J. 239 (2014) 93–104, https://doi.org/10.1016/j.cej.2013.11.013.
[21] R. Epsztein, O. Nir, O. Lahav, M. Green, Selective nitrate removal from groundwater using a hybrid nanofiltration–reverse osmosis filtration scheme, Chem. Eng. J. 279 (2015) 372–378, https://doi.org/10.1016/j.cej.2015.05.010.
[22] H. Niu, Z. Zhang, X. Wang, X. Wan, C. Shao, Y. Guo, Theoretical insights into the mechanism of selective nitrate-to-ammonia electroreduction on single-atom catalysts, Adv. Funct. Mater. 31 (2020) 2008533, https://doi.org/10.1002/adfm.202008533.
[23] X. Zhang, Y. Wang, C. Liu, Y. Yu, S. Lu, B. Zhang, Recent advances in non-noble metal electrocatalysts for nitrate reduction, Chem. Eng. J. 403 (2021), 126269, https://doi.org/10.1016/j.cej.2020.126269.
[24] J. Li, G. Zhan, J. Yang, F. Quan, C. Mao, Y. Liu, B. Wang, F. Lei, L. Li, A.W.M. Chan, L. Xu, Y. Shi, Y. Du, W. Hao, P.K. Wong, J. Wang, S.X. Dou, L. Zhang, J.C. Yu, Efficient ammonia electrosynthesis from nitrate on strained ruthenium nanoclusters, J. Am. Chem. Soc. 142 (2020) 7036–7046, https://doi.org/10.1021/jacs.0c00418.
[25] H. Yin, Z. Chen, S. Xiong, J. Chen, C. Wang, R. Wang, Y. Kuwahara, J. Luo, H. Yamashita, Y. Peng, J. Li, Alloying effect-induced electron polarization drives nitrate electroreduction to ammonia, Chem. Catal. 1 (2021) 1088–1103, https://doi.org/10.1016/j.checat.2021.08.014.
[26] S. Guo, H. Li, K.N. Heck, X. Luan, W. Guo, G. Henkelman, M.S. Wong, Gold boosts nitrate reduction and deactivation resistance to indium-promoted palladium catalysts, Appl. Catal. B: Environ. 305 (2022), 121048, https://doi.org/10.1016/j.apcatb.2021.121048.
[27] Y. Zhang, X. Chen, W. Wang, L. Yin, J.C. Crittenden, Electrocatalytic nitrate reduction to ammonia on defective Au1Cu (111) single-atom alloys, Appl. Catal. B: Environ. 310 (2022), 121346, https://doi.org/10.1016/j.apcatb.2022.121346.
[28] Y. Xu, K. Ren, T. Ren, M. Wang, M. Liu, Z. Wang, X. Li, L. Wang, H. Wang, Cooperativity of Cu and Pd active sites in CuPd aerogels enhances nitrate electroreduction to ammonia, Chem. Comm. 57 (2021) 7525–7528, https://doi.org/10.1039/d1cc02105b.
[29] X. Fu, X. Zhao, X. Hu, K. He, Y. Yu, T. Li, Q. Tu, X. Qian, Q. Yue, M.R. Wasielewski, Y. Kang, Alternative route for electrochemical ammonia synthesis by reduction of nitrate on copper nanosheets, Appl. Mater. Today 19 (2020), 100620, https://doi.org/10.1016/j.apmt.2020.100620.
[30] Y. Xu, M. Wang, K. Ren, T. Ren, M. Liu, Z. Wang, X. Li, L. Wang, H. Wang, Atomic defects in pothole-rich two-dimensional copper nanoplates triggering enhanced electrocatalytic selective nitrate-to-ammonia transformation, J. Mater. Chem. A 9 (2021) 16411–16417, https://doi.org/10.1039/d1ta04743d.
[31] G.A. Cerrón-Calle, A.S. Fajardo, C.M. Sánchez-Sánchez, S. Garcia-Segura, Highly reactive Cu-Pt bimetallic 3D-electrocatalyst for selective nitrate reduction to ammonia, Appl. Catal. B: Environ. 302 (2022), 120844, https://doi.org/10.1016/j.apcatb.2021.120844.
[32] Z. Gong, W. Zhong, Z. He, Q. Liu, H. Chen, D. Zhou, N. Zhang, X. Kang, Y. Chen, Regulating surface oxygen species on copper (I) oxides via plasma treatment for effective reduction of nitrate to ammonia, Appl. Catal. B: Environ. 305 (2022), 121021, https://doi.org/10.1016/j.apcatb.2021.121021.
[33] Y. Xu, K. Ren, T. Ren, M. Wang, Z. Wang, X. Li, L. Wang, H. Wang, Ultralow-content Pd in-situ incorporation mediated hierarchical defects in corner-etched Cu_2O octahedra for enhanced electrocatalytic nitrate reduction to ammonia, Appl. Catal. B Environ. 306 (2022), 121094, https://doi.org/10.1016/j.apcatb.2022.121094.
[34] T. Ren, Z. Yu, H. Yu, K. Deng, Z. Wang, X. Li, H. Wang, L. Wang, Y. Xu, Interfacial polarization in metal-organic framework reconstructed $Cu/Pd/CuO_x$ multi-phase heterostructures for electrocatalytic nitrate reduction to ammonia, Appl. Catal. B Environ. 318 (2022), 121805, https://doi.org/10.1016/j.apcatb.2022.121805.
[35] T. Ren, K. Ren, M. Wang, M. Liu, Z. Wang, H. Wang, X. Li, L. Wang, Y. Xu, Concave-convex surface oxide layers over copper nanowires boost electrochemical nitrate-to-ammonia conversion, Chem. Eng. J. 426 (2021), https://doi.org/10.1016/j.cej.2021.130759.
[36] Q. Xue, H. Huang, J.-Y. Zhu, Y. Zhao, F.-M. Li, P. Chen, Y. Chen, Au@Rh core-shell nanowires for hydrazine electrooxidation, Appl. Catal. B: Environ. 278 (2020), https://doi.org/10.1016/j.apcatb.2020.119269.
[37] J.X. Feng, L.X. Ding, S.H. Ye, X.J. He, H. Xu, Y.X. Tong, G.R. Li, Co(OH)2 @PANI Hybrid Nanosheets with 3D Networks as High-Performance Electrocatalysts for Hydrogen Evolution Reaction, Adv. Mater. 27 (2015) 7051–7057, https://doi.org/10.1002/adma.201503187.
[38] Y. Peng, Q. Liu, B. Lu, T. He, F. Nichols, X. Hu, T. Huang, G. Huang, L. Guzman, Y. Ping, S. Chen, Organically capped iridium nanoparticles as high-performance bifunctional electrocatalysts for full water splitting in both acidic and alkaline media: impacts of metal–ligand interfacial interactions, ACS Catal. 11 (2021) 1179–1188, https://doi.org/10.1021/acscatal.0c03747.
[39] Y. Shi, Y. Ji, J. Long, Y. Liang, Y. Liu, Y. Yu, J. Xiao, B. Zhang, Unveiling hydrocerussite as an electrochemically stable active phase for efficient carbon dioxide electroreduction to formate, Nat. Commun. 11 (2020) 3415, https://doi.org/10.1038/s41467-020-17120-9.
[40] Y. Xu, X. Li, J. Gao, J. Wang, G. Ma, X. Wen, Y. Yang, Y. Li, M. Ding, A hydrophobic FeMn@Si catalyst increases olefins from syngas by suppressing C1 by-products, Science 371 (2021) 610–613, https://doi.org/10.1126/science.abb3649.
[41] Q. Xue, J. Bai, C. Han, P. Chen, J.-X. Jiang, Y. Chen, Au nanowires@Pd-polyethylenimine nanohybrids as highly active and methanol-tolerant electrocatalysts toward oxygen reduction reaction in alkaline media, ACS Catal. 8 (2018) 11287–11295, https://doi.org/10.1021/acscatal.8b03447.
[42] Y. Wang, S. Chen, S. Zhao, Q. Chen, J. Zhang, Interfacial coordination assembly of tannic acid with metal ions on three-dimensional nickel hydroxide nanowalls for efficient water splitting, J. Mater. Chem. A 8 (2020) 15845–15852, https://doi.org/10.1039/d0ta02229b.
[43] S. Yin, S. Liu, S. Jiao, H. Zhang, Y. Xu, Z. Wang, X. Li, L. Wang, H. Wang, Tannic acid decorated AuPd lavender-like nanochains for enhanced oxygen reduction electrocatalysis, J. Mater. Chem. A 9 (2021) 15678–15683, https://doi.org/10.1039/d1ta04114b.
[44] H. Xu, T. Liu, S. Bai, L. Li, Y. Zhu, J. Wang, S. Yang, Y. Li, Q. Shao, X. Huang, Cation exchange strategy to single-atom noble-metal doped CuO nanowire arrays with ultralow overpotential for H_2O splitting, Nano Lett. 20 (2020) 5482–5489, https://doi.org/10.1021/acs.nanolett.0c02007.
[45] Z. Duan, K. Deng, C. Li, M. Zhang, Z. Wang, Y. Xu, X. Li, L. Wang, H. Wang, Polyaniline-coated mesoporous Rh films for nonacidic hydrogen evolution reaction, Chem. Eng. J. 428 (2022), https://doi.org/10.1016/j.cej.2021.132646.
[46] J.X. Feng, S.Y. Tong, Y.X. Tong, G.R. Li, Pt-like hydrogen evolution electrocatalysis on PANI/CoP hybrid nanowires by weakening the shackles of hydrogen ions on the surfaces of catalysts, J. Am. Chem. Soc. 140 (2018) 5118–5126, https://doi.org/10.1021/jacs.7b12968.
[47] F. Meng, Y. Yu, D. Sun, S. Lin, X. Zhang, T. Xi, C. Xu, H. OuYang, W. Chu, L. Shang, Q. Su, B. Xu, Three-dimensional needle branch-like PANI/CoNiP hybrid

electrocatalysts for hydrogen evolution reaction in acid media, ACS Appl. Energy Mater. 4 (2021) 2471–2480, https://doi.org/10.1021/acsaem.0c03033.
[48] S. Ashokan, V. Ponnuswamy, P. Jayamurugan, Synthesis and characterization of CuO nanoparticles, DBSA doped PANI and PANI/DBSA/CuO hybrid composites for diode and solar cell device development, J. Alloy. Compd. 646 (2015) 40–48, https://doi.org/10.1016/j.jallcom.2015.05.088.
[49] B. Gangaja, S. Chandrasekharan, S. Vadukumpully, S.V. Nair, D. Santhanagopalan, Surface chemical analysis of CuO nanofiber composite electrodes at different stages of lithiation/delithiation, J. Power Sources 340 (2017) 356–364, https://doi.org/10.1016/j.jpowsour.2016.11.087.
[50] T. Wang, X. Zhang, X. Zhu, Q. Liu, S. Lu, A.M. Asiri, Y. Luo, X. Sun, Hierarchical CuO@ZnCo LDH heterostructured nanowire arrays toward enhanced water oxidation electrocatalysis, Nanoscale 12 (2020) 5359–5362, https://doi.org/10.1039/d0nr00752h.
[51] J. Li, Y. Ren, Z. Ren, S. Wang, Y. Qiu, J. Yu, Aligned polyaniline nanowires grown on the internal surface of macroporous carbon for supercapacitors, J. Mater. Chem. A 3 (2015) 23307–23315, https://doi.org/10.1039/c5ta05381a.
[52] D. Wang, L. Yang, H. Liu, D. Cao, Polyaniline-coated Ru/Ni$(OH)_2$ nanosheets for hydrogen evolution reaction over a wide pH range, J. Catal. 375 (2019) 249–256, https://doi.org/10.1016/j.jcat.2019.06.008.
[53] J. Zhang, Y. Li, Z. Wang, Y. Wang, F. Wang, M. Chen, Three-dimensionally hierarchical NiCoP@PANI architecture for high-performance hydrogen evolution reaction, Nanotechnology 31 (2020), 445401, https://doi.org/10.1088/1361-6528/aba7e1.
[54] H. Xu, Y. Ma, J. Chen, W.X. Zhang, J. Yang, Electrocatalytic reduction of nitrate - a step towards a sustainable nitrogen cycle, Chem. Soc. Rev. 51 (2022) 2710–2758, https://doi.org/10.1039/d1cs00857a.
[55] Y. Xu, X. Chai, T. Ren, S. Yu, H. Yu, Z. Wang, X. Li, L. Wang, H. Wang, Ir-Doped Ni-based metal-organic framework ultrathin nanosheets on Ni foam for enhanced urea electro-oxidation, Chem. Comm. 56 (2020) 2151–2154, https://doi.org/10.1039/c9cc09484a.
[56] Y. Xu, M. Liu, M. Wang, T. Ren, K. Ren, Z. Wang, X. Li, L. Wang, H. Wang, Methanol electroreforming coupled to green hydrogen production over bifunctional NiIr-based metal-organic framework nanosheet arrays, Appl. Catal. B Environ. 300 (2022), 120753, https://doi.org/10.1016/j.apcatb.2021.120753.
[57] Y. Xu, M. Liu, S. Wang, K. Ren, M. Wang, Z. Wang, X. Li, L. Wang, H. Wang, Integrating electrocatalytic hydrogen generation with selective oxidation of glycerol to formate over bifunctional nitrogen-doped carbon coated nickel-molybdenum-nitrogen nanowire arrays, Appl. Catal. B: Environ. 298 (2021), 120493, https://doi.org/10.1016/j.apcatb.2021.120493.
[58] D. Cao, H. Xu, D. Cheng, Branch-leaf-shaped CuNi@NiFeCu nanodendrites as highly efficient electrocatalysts for overall water splitting, Appl. Catal. B: Environ. 298 (2021), 120600, https://doi.org/10.1016/j.apcatb.2021.120600.
[59] H. Liang, L. Zhang, H. Wu, Exploration of twin-modified grain boundary engineering in metallic copper predominated electromagnetic wave absorber, Small (2022), e2203620, https://doi.org/10.1002/smll.202203620.
[60] Y. Wang, W. Zhou, R. Jia, Y. Yu, B. Zhang, Unveiling the activity origin of a copper-based electrocatalyst for selective nitrate reduction to ammonia, Angew. Chem. Int. Ed. 59 (2020) 5350–5354, https://doi.org/10.1002/anie.201915992.
[61] K.P. Kuhl, E.R. Cave, D.N. Abram, T.F. Jaramillo, New insights into the electrochemical reduction of carbon dioxide on metallic copper surfaces, Energy Environ. Sci. 5 (2012) 7050, https://doi.org/10.1039/c2ee21234j.
[62] A. Herath, C. Reid, F. Perez, C.U. Pittman Jr., T.E. Mlsna, Biochar-supported polyaniline hybrid for aqueous chromium and nitrate adsorption, J. Environ. Manag. 296 (2021), 113186, https://doi.org/10.1016/j.jenvman.2021.113186.
[63] S. Wang, M. Zhang, J. Feng, T. Wei, Y. Ren, J. Ma, In-situ polymerization of polyaniline modified by phosphotungstic acid on the surface of hollow carbon for two-way efficient reduction of nitrate in water, Chem. Eng. J. 430 (2022), 133175, https://doi.org/10.1016/j.cej.2021.133175.
[64] H. Wang, W. Wang, H. Yu, Q. Mao, Y. Xu, X. Li, Z. Wang, L. Wang, Interface engineering of polyaniline-functionalized porous Pd metallene for alkaline oxygen reduction reaction, Appl. Catal. B Environ. 307 (2022), 121172, https://doi.org/10.1016/j.apcatb.2022.121172.